

Full Length Article

Surface reactions of ethanol on UO₂ thin film. Dehydrogenation and dehydration pathwaysHicham Idriss^{a,c,*}, Thomas Gouder^b^a Institute of Functional Interfaces (IFG), Karlsruhe Institute of Technology (KIT), Karlsruhe, Germany^b Joint Research Centre (JRC), European Commission (EC), Germany^c Department of Chemistry, University College London (UCL), London, UK

ARTICLE INFO

Keywords:

Uranium dioxide
 Temperature Programmed Desorption (TPD)
 Ethanol-TPD
 Ethanol dehydration
 Ethanol dehydrogenation
 Activation energy of desorption

ABSTRACT

The reaction of ethanol has been investigated on a UO₂ thin film by temperature programmed desorption. Two channels for ethanol desorption are identified. The first, in the 250–500 K region, is coverage dependent while the second with a maximum peak temperature (T_p) at ca. 630 K is not. The desorption energy, E_d , of the second channel is found to be equal to ca. 150 kJ/mol with a prefactor of 10^{12} s^{-1} and a desorption order $n = 2$. This is attributed to surface ethoxides re-combinative desorption. This second desorption channel is accompanied by the desorption of acetaldehyde (and hydrogen) and ethylene (and water). Acetaldehyde (CH₃CHO) desorption, produced by the dehydrogenation of ethoxides, was sensitive to surface coverage. Its T_p changed from 640 K at $\theta = 0.06$ to 610 K at $\theta = 1$, while ethylene (CH₂=CH₂) desorption T_p , produced by the dehydration of ethoxides did not shift. The molar ratio of these two products (CH₃CHO/CH₂=CH₂) of 0.8 is similar to that previously found on a UO₂(1 1 1) single crystal and fits with the U–O bonding nature that contains a non-negligible fraction of covalency.

1. Introduction

The surface reaction of metal oxides with organic adsorbates is part of many processes extending from catalysis [1], to sensors [2], to medical implants [3], and environmental remediation applications [4]. It can be grouped into two categories: acid-base and oxidation–reduction (redox) reactions. In the first, for simplicity in the case of a binary metal oxide, a surface metal cation acts as a Lewis acid site, and a surface oxygen anion as a Lewis base site. This reaction is often followed by another one that involves an oxidation/reduction step depending on the degree of reduction of the metal cation. The dehydrogenation of isobutane to isobutene over Cr oxide-based catalysts [5] and the three-way automobile converters on CeO₂-based catalysts [6] are among many known examples. The reasons for this second step (redox reaction) are not trivial as they involve electron transfer from and/or to the surface. One of the simplest methods to probe into this property is to use a molecule that can be oxidized easily, such as a linear alcohol. In this case, oxidation means the removal of two hydrogen ions and two electrons. For example, a methanol molecule (CH₃OH) is oxidized to formaldehyde (HCHO) and hydrogen molecules over Cu [7]- or Ag [8]-based catalysts. In general, on metals the main reaction is

dehydrogenation to the aldehyde that is often followed by their decomposition. For example, in the case of ethanol, it reacts on Ni surfaces to give acetaldehyde and hydrogen [9,10]. Acetaldehyde is further decomposed to CH₄ and CO. On metal oxides there is however a selectivity issue because the removal of these hydrogen atoms can be accomplished by the removal of an oxygen atom from the same molecule or from the surface. This is best described by an ethanol molecule as it involves still a unimolecular reaction. While the dehydrogenation reaction yields acetaldehyde (CH₃CHO) and H₂ the dehydration gives ethylene (CH₂ = CH₂) and a molecule of water. The extent of both reactions is dictated by the electronic and structural properties of the metal oxide [11].

Uranium oxides may offer a rich template for this type of investigation because it can accommodate different oxidation states in different metastable phases [12]. One of the most stable uranium oxides is UO₂ and while there are previous studies addressing its surface reaction our knowledge of its activity still lags that of early transition metal oxides because the latter are often used as a catalyst while the former, because of its radioactivity, is not. However, more information on its possible reactions with the surrounding would help designing optimal long-term storage environment [13]. For example, some of the

* Corresponding author at: Institute of Functional Interfaces (IFG), Karlsruhe Institute of Technology (KIT), Karlsruhe, Germany.

E-mail addresses: hicham.idriss@kit.edu, h.idriss@ucl.ac.uk (H. Idriss).

storage environments recommended to track the quality of uranium oxides micro-particles are ethanol-based [14]. Moreover, as it is one of a few compounds with the valence band composed of f-electrons (Mott insulator [15]) it offers some chemical pathways not encountered by the earlier transition metal cations. For example, organometallic compounds of U^{3+} have shown some unique carbonyl coupling activity [16]. Also, the high coordination number of U cations may result in the formation of double coordinative unsaturation that can accommodate two adsorbates per a metal cation site and this when combined with the ease of removal of an oxygen atom [17] has been shown in the case of β - UO_3 to drive oxidative coupling of acetylene to furan [18].

In this work, a thin film of UO_2 that is [1 1 1] oriented [19] is prepared and studied for the reaction of a representative primary alcohol (ethanol) by temperature programmed desorption to compare its activity to a previously studied similar reaction on a $UO_2(1\ 1\ 1)$ single crystal [20] and other oxides. In a previous work the reaction of ethanol was studied at a full monolayer coverage over a $UO_2(1\ 1\ 1)$ single crystal [20]. It was found that both reactions products were formed (acetaldehyde and ethylene) with a molecular ratio of 0.8. Among the objectives of the work are the extraction of the desorption energies, the extent of dissociative versus molecular adsorption and the relative selectivity of the dehydrogenation (to acetaldehyde and H_2) to the dehydration (to ethylene and water) reaction products with surface coverage.

2. Experimental

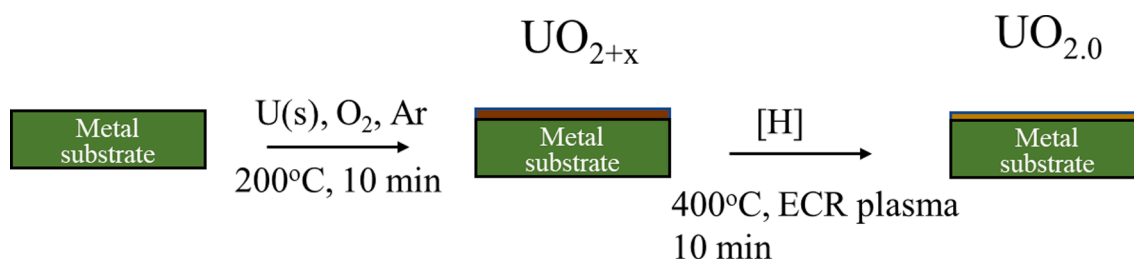
A UO_{2+x} ($x < ca. 0.1$) thin film, before being converted to stoichiometric UO_2 , was synthesized by reactive direct-current (dc) sputtering from a uranium target. The sputter gases used were Ar and O_2 . The film was deposited on a gold stainless-steel substrate, prior cleaned by Ar ion sputtering, followed by annealing to 200 °C for 10 min. The plasma in the diode source was maintained by injection of 25–50 eV energy electrons allowing operation at low pressures. After film formation and to produce a stoichiometric $UO_{2.0}$ the initial film was exposed to atomic hydrogen produced with an Electron Cyclotron Resonance (ECR) plasma source at 400 °C for 10 min. This eliminated surplus oxygen leaving $UO_{2.0}$.

Thin film deposition, plasma treatment, gas exposures, and all data acquisition equipment were carried out in situ and all chambers (growth and spectroscopy) are interconnected. The background pressure was lower than 3×10^{-10} torr. Low temperatures were reached by cooling down the sample holder stage made of copper using liquid nitrogen.

spectrometers were calibrated by using metallic $Au-4f_{7/2}$ at 84.0 eV BE for XPS and the Fermi edges for the UPS. The binding energy reported are as acquired (samples were not biased) because no shift in the spectra was seen. This was based on the $O1s$ binding energy line (of UO_2) centered at 530.5 eV in the case of XPS and the $U5f$ line in the case of UPS. A typical pressure for XPS during data acquisition was $2\text{--}3 \times 10^{-10}$ torr and during UPS (He II) was $1\text{--}2 \times 10^{-9}$ torr.

The TPD system is equipped with a Hiden quadrupole mass spectrometer (HAL 8 RC RGA) that monitors up to 200 amu. The mass spectrometer head is enclosed in a stainless-steel cone with an orifice of about 3 mm in diameter pumped by a turbomolecular pump at a pressure lower than 3×10^{-10} torr. The TPD chamber base pressure is pumped with a turbomolecular pump and a Ti sublimation pump giving a base pressure of about 2×10^{-10} torr or lower. A typical run consisted of introducing ethanol vapour via a leak valve (from a dosing line) into the chamber reaching a pressure ranging between 10^{-9} and 10^{-8} torr for x seconds depending on the needed exposure; between 0.15 L and 7 L ($1L = 10^{-6}$ torr.s). Most runs consisted of monitoring 13 masses (m/e 2, 16, 18, 25, 26, 27, 28, 29, 31, 43, 44, 45, and 46) to cover hydrogen, water, CO, ethylene, acetaldehyde, ethanol, and CO_2 desorptions. Ramping rate 1.2 K/s. Ethanol was put into a glass-to-metal bulb that was connected to a stainless-steel dosing line and pumped with a scroll pump at a base pressure of about 4×10^{-2} torr. Ethanol was cleaned prior to dosing by freeze–thaw pump cycles to remove water and CO_2 . Before dosing ethanol, the surface was cleaned by heating in UHV to about 550 °C multiple times (for about 10 min each). After ethanol was dosed onto the surface of UO_2 , at a given temperature, the chamber was pumped down to a pressure below 10^{-9} torr prior to starting the TPD run. This took about 30–45 min. The distance between the orifice of the mass spectrometer and the surface was about 1 mm.

Qualitative analysis was conducted by calculating the area of the mass spectrum cracking patterns of each desorbing fragment. The overlapping peaks in the case of multiple desorption features (such as in the case of ethanol, acetaldehyde, and ethylene) were removed using the same deconvolution procedure described numerous times before [21]. The Origin Pro 2018 SR1 software was used for curve fitting and peak integration. The area under each curve was corrected by the mass spectrometer sensitivity factor, which was calculated using the method reported by Ko et al.[22]. Carbon yield and selectivity were calculated using the method reported previously by Sheng et al.[23]. The order of reaction and desorption energy were determined using the Arrhenius plot [24] and by non-linear model fitting (regression analysis) of the Polanyi–Wigner (PW) equation [25]. The non-linear regression analysis



UPS spectra were taken with He II (40.81 eV) UV light, produced by a high-intensity windowless discharge lamp. XPS spectra were recorded using monochromatized Al $K\alpha$ (1486.6 eV) radiation, produced by a SPECS μ -focus source. Photoelectrons energies were analyzed using a Specs Phoibos 150 hemispherical analyzer. The photons power used was 120 W (12 kV, 10 mA), and a typical spectrum was conducted with 20 eV pass energy at 0.05 eV/step (0.65 s/step). Prior to measurements the

(model fitting) was done using the “Solver” add-in in the Microsoft Excel spreadsheet. Mass spectrometer correction factors with respect to mass 28 in the chamber were as follows. Ethanol (m/e 31 = 2.1), acetaldehyde (m/e 29 = 2.6), ethylene (m/e 26 = 3.6) and CO_2 (m/e 44 = 1.3).

UV–vis absorbance measurements were conducted in transmission mode using a Cary 5000 UV–Vis–NIR spectrometer. The UO_2 thin film in this case was grown on a quartz sample holder that was prior cleaned by Ar ion sputtering and annealing and the quality of the film was checked by XPS $U4f$ using a 0.3 eV charge neutralizer because of the insulating

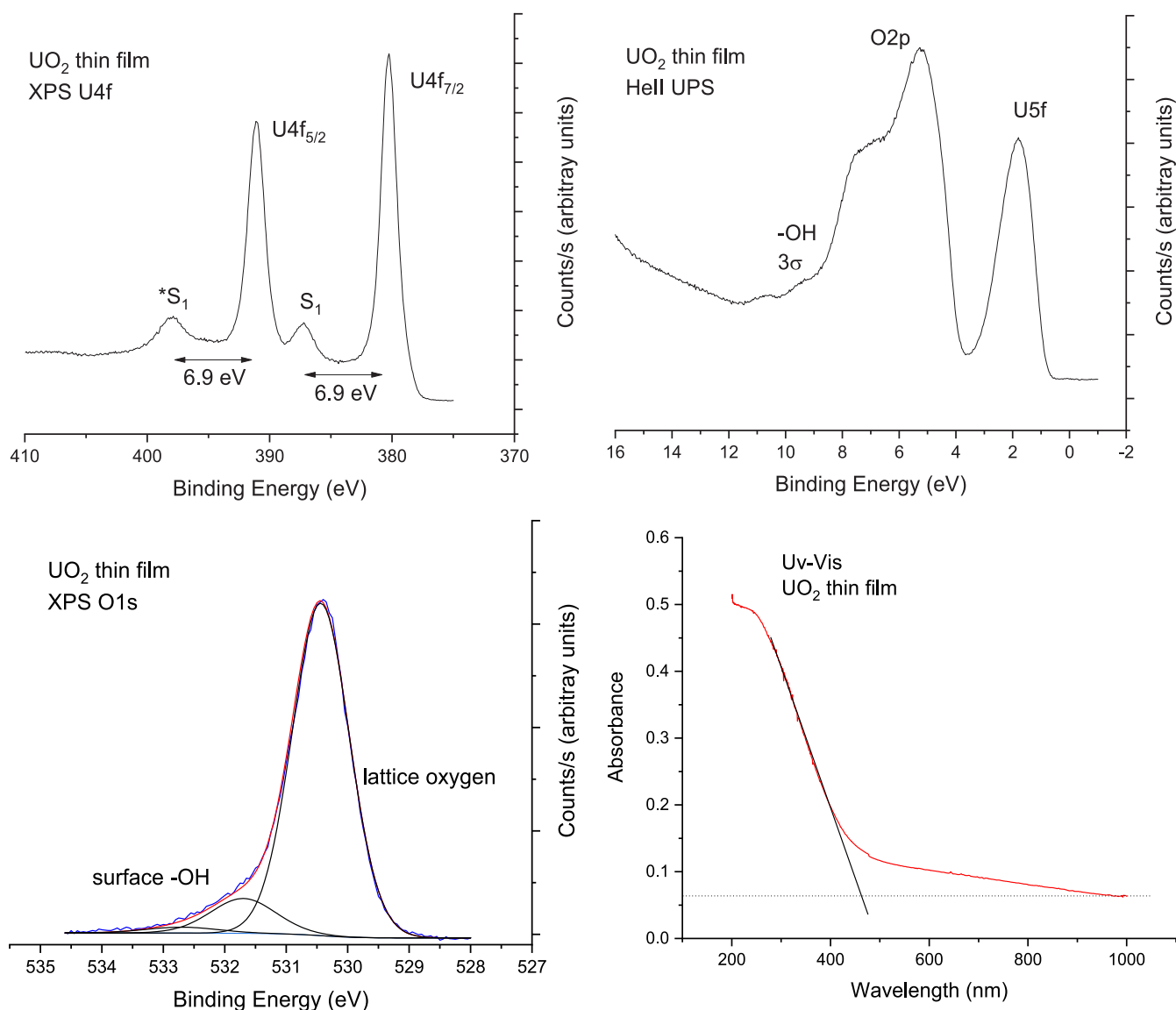


Fig. 1. A. XPS U4f of a UO_2 thin film. B. UPS He(II) of a UO_2 thin film. C. XPS O1s of a UO_2 thin film. D. UV-vis absorbance of a UO_2 thin film prepared on a quartz support (transmission mode).

nature of quartz.

3. Results and discussion

Fig. 1A presents XPS U4f of the UO_2 thin film. The core and valence band electronic structure differences between UO_2 (U^{4+}), U_2O_5 (U^{5+}), and UO_3 (U^{6+}) were recently outlined in one of our last studies [26]. The main peaks at binding energies of 380.0 and 391.0 eV are due to $\text{U}4f_{7/2}$ and $\text{U}4f_{5/2}$ spin-orbit splitting of U cations, respectively. Assessment of the oxidation state is based on several factors: (i) the binding energy of these lines, (ii) the presence of a satellite peak 6.9 eV after each main line, and (iii) the ratio of the satellite to the main peak. All these together point to a stoichiometric or near stoichiometric surface where U cations are in the +4-oxidation state. The valence band (He(II) UPS) is given in Fig. 1B. It shows a pronounced $\text{U}5f$ signal with a full-width half maximum (FWHM) of 1.5 eV at about 1.7–1.8 eV below E_F . Its peak area is about 24 % of that of the $\text{O}2p$. This is considerably different from the valence band of U_2O_5 (where the $\text{U}5f$ peak area represents about 0.08 of that of the $\text{O}2p$). There is also, the unavoidable presence of surface hydroxyls (the σ OH signal at about 10 eV) and probably irreversibly adsorbed water just after (1b2 orbital) [27]. XPS O1s shows the lattice O

at 530.5 eV and surface hydroxyls at about 531.7 eV (Fig. 1C)[28]. UO_2 is a Mott insulator [12], in other words, it is not a semiconductor in the common description. Its conductivity is due to electron hopping within the f-band and with an energy barrier of about 2 eV. However, this conducting property is very sensitive to its stoichiometry. In general, it shows n-type characteristics for sub-stoichiometric UO_{2-x} (which is largely unstable) and p-type super-stoichiometric UO_{2+x} , which is more common [29,30]. Fig. 1D presents the UV-Vis absorbance of a UO_2 thin film prepared over a quartz slide in transmission mode. To estimate the film thickness we relied on the Si2p XPS signal of the quartz substrate to prepare a film thin enough for transmission, the film's estimated thickness is about 20 nm. The extracted band gap is found to be about 2.5 eV. The extraction of the band gap energy using this method has a non-negligible % of error because of the baseline of the spectrum, so this band gap energy is approximative and is most likely that of UO_{2+x} ; measurements were conducted ex-situ about one week after the film was prepared. Still, it attests of the bulk quality of the oxide that is in line with previous reported measurements [31].

Fig. 2 (A and B) displays a representative data of ethanol-TPD on a UO_2 thin film at a 2L exposure (ramping rate, $\beta = 1.2$ K/s) which is near surface saturation (surface coverage effect is shown in Fig. 3). The main

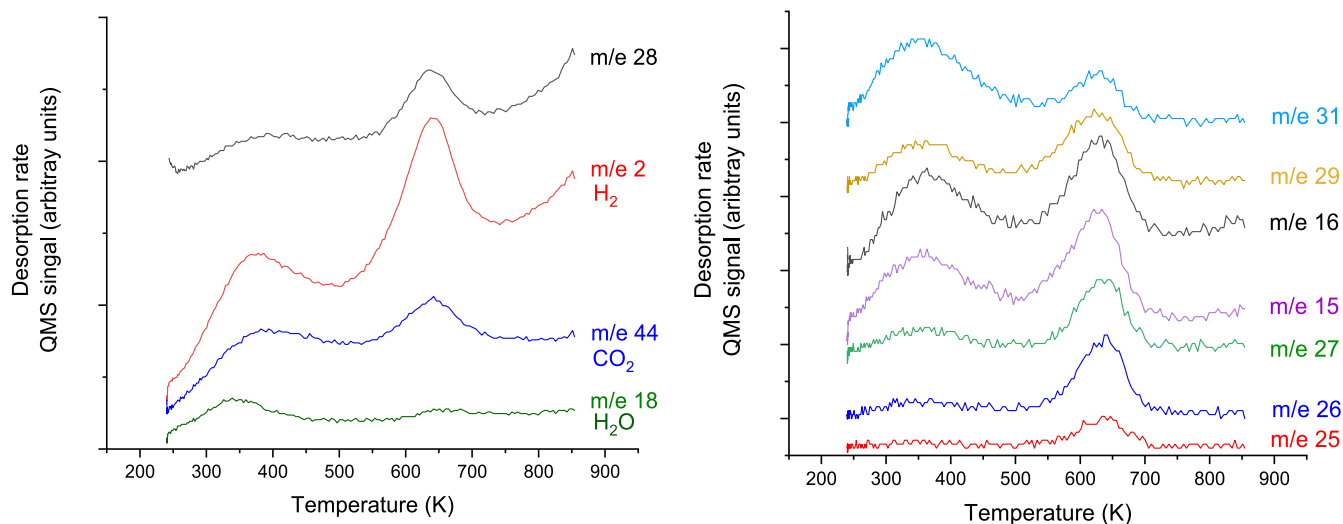


Fig. 2. A. Non-subtracted products distribution during ethanol-TPD on a UO_2 thin film. B. Non-subtracted products distribution during ethanol-TPD on a UO_2 thin film. m/e 25, 26, and 27 are for ethylene. m/e 15 and 16 are for methane, m/e 29 is for acetaldehyde, and m/e 31 is for ethanol.

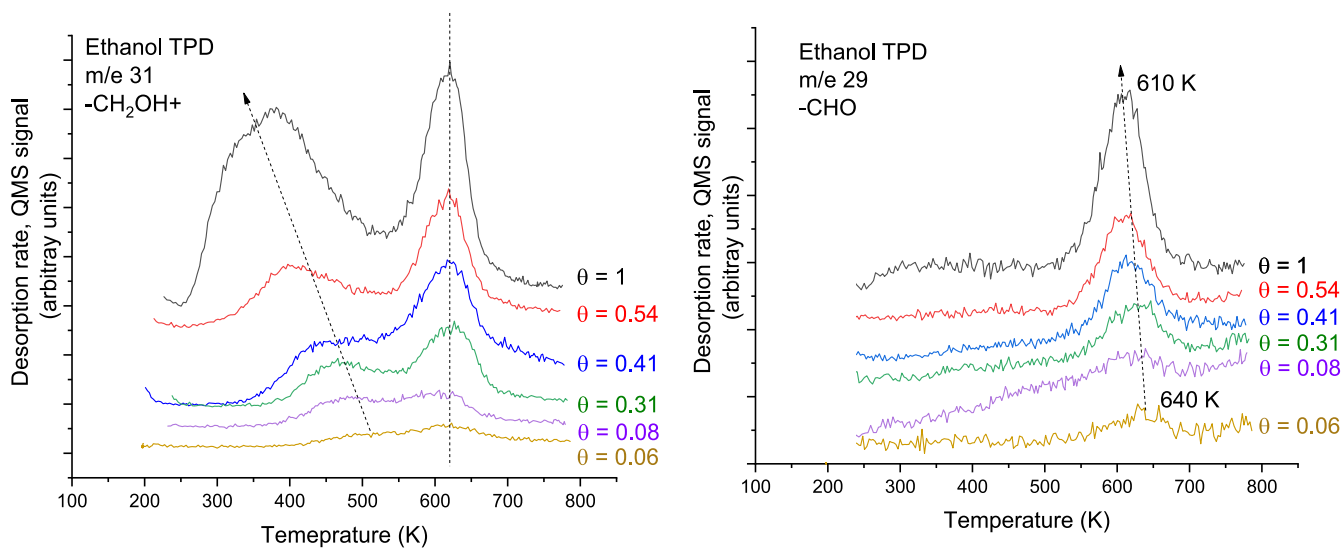


Fig. 3. A. Ethanol desorption as a function of surface coverage during ethanol-TPD of a UO_2 thin film. B. Acetaldehyde desorption as a function of surface coverage during ethanol-TPD of a UO_2 thin film.

nonhydrocarbon fragments are given in Fig. 2A. These are m/e 28, m/e 44, m/e 2 and m/e 18 desorbing in two different domains, one in the 250–450 K range and the other in the 550–750 K range. The spectra are as-recorded with no subtraction due to the contribution of other fragments. After quantitative analysis, it was found that all m/e 28 and the second m/e 44 are from the fragmentation patterns of other hydrocarbons (see below) while m/e 2 and m/e 18 are due to hydrogen and water. Note the desorption of water in the second channel too (as shown below it is due to the dehydration reaction to ethylene). Fig. 2B shows the desorption of masses related to hydrocarbons. These are attributed

Table 1
Fraction of compounds desorbing during ethanol-TPD over a UO_2 thin film.

Reactant, product	250–450 K	550–750 K
Ethanol	0.28	0.12
Acetaldehyde	0.07	0.25
Ethylene	0.13	0.34
Methane	0.25	0.29
Carbon dioxide	0.27	traces

to four different compounds. m/e 31 is due to unreacted ethanol (m/e 45 and m/e 46 are present with the same shape and temperature range, not shown for simplicity). m/e 29 is largely due to acetaldehyde, the dehydrogenation product. Part of m/e 29 is due to ethanol (about 35 % of m/e 31). m/e 15, and m/e 16 are largely due to methane and m/e 25, 26 and 27 are due to ethylene desorption (the dehydration product of ethanol). These products also desorb in two temperature domains, like those of Fig. 2A. It is important to note that acetaldehyde and ethylene are exclusively desorbed at the high-temperature domain. There is also the desorption of methane (m/e 15 and m/e 16). Methane (and CO_2) can be formed via the partial reforming of ethanol ($\text{CH}_3\text{CH}_2\text{OH} + \text{H}_2\text{O} \rightarrow \text{CH}_4 + \text{CO}_2 + 2\text{H}_2$). In this work we have not further studied this reaction; because of its complexity it may not be solely addressed by TPD. Table 1 presents the molar selectivity of carbon-containing compounds defined as the fraction of the mass spectrometer corrected desorption of product, i , over the sum of all products including the reactant (ethanol).

Fig. 3 (A and B) presents the coverage effect on ethanol desorption as tracked by its m/e 31. It is assumed that full coverage was obtained at the largest peak areas from which the fractional coverage was obtained

as indicated. There are two main observations.

1. The first peak shifts to a lower temperature with increasing coverage while the second peak does not.
2. Peak area analysis indicated that within experimental errors both peaks increase together with no noticeable preference.

The second point indicates that the high-temperature peak is not due to adsorption on a high-energy site otherwise it would have populated first, such as in the case for example of ethanol adsorbed on an oxygen defect site on reduced TiO₂ single crystals [32,33]. However, the fact that only the desorption temperature maximum of the first peak is affected by surface coverage means that the second desorption is less sensitive to repulsive interaction (destabilizing its energy state); if repulsive interaction is the cause. It is possible that the first peak is complex and originates from two different species: a molecularly adsorbed species that is more sensitive to surface coverage and during the temperature ramping the energy needed to dissociate it to ethoxides is gained. Because a good fraction of the adsorbed species would by then have desorbed the remaining dissociated ethanol (ethoxide species, CH₃CH₂O(a)) would not be interacting. There are no computational studies of primary alcohols on UO₂ surfaces. The distance between two U⁴⁺ cations, of the (1 1 1) terminated surface, for example, the most stable fluorite surface, is 3.8 Å which is smaller than the van der Waals size of an ethanol molecule (about 5 Å) [34]. Fig. 2A shows that a large fraction of water desorbed at the first peak temperature, this desorption is attributed to a re-combinative reaction between two surface hydroxyls. This would free surface sites for ethanol dissociation since an ethanol dissociation to ethoxides needs two sites (a uranium cation and an oxygen anion) to make surface hydroxyls and ethoxides as presented by equations 1 and 2.

Water desorption



dissociated water *water desorption + site regeneration*

–U–O– represents the sites for the dissociative adsorption and (g) represents gas.

Ethanol dissociative adsorption



molecular ethanol *dissociated ethanol (ethoxide)*

–U–O– represents the sites for the dissociative adsorption and (g) represents gas.

To further study this, one set of the ethanol desorption profiles, at $\theta = 0.54$ ($\beta = 1.2$ K/s), after being separated into two distinct peaks is further analyzed. The desorption was simulated knowing that its rate can be expressed as (equation (3))

Table 2

Extracted kinetic parameters for both ethanol desorption peaks during TPD.

	E (kJ/mol)	k_o (s ⁻¹)	n
Peak 1 (400 K)	90	10 ¹²	2
Peak 2 (620 K)	150	10 ¹²	2

$$\text{desorption rate, } r = -\frac{d\theta}{dT} = \frac{k_o \theta^n \exp\left(\frac{-E_d}{RT}\right)}{\beta_H} \quad (3)$$

Where θ is the surface coverage, β_H is the heat rate = 1.2 K s^{-1} , E_d is the desorption energy in J/mol, R is perfect gas constant $8.414 \text{ J/mol K}^{-1}$, k_o is the prefactor in s⁻¹ and T is temperature in K. Analytical simulation of the equation with the experimental desorption rate while varying the desorption energy and prefactor was conducted. Table 2 presents the values for the best fit for E_d and k_o for $n = 2$ and $\theta = 0.54$.

To extract the desorption order, n , a plot of $\ln(r/\theta^n)$ as a function of $1/T$ would give a straight line for a given order of desorption for both peaks separately (Fig. 4). Peak 2 showed a clear linear trend with $n = 2$. Peak 1 however was not sensitive to the order of desorption in the relevant desorption domain and could be equally modelled by $n = 1$ or 2. The change in its desorption temperature as a function of coverage is given in Table 3 (and Fig. 5). The simulation was conducted for $n = 1$ and $n = 2$ separately. The desorption energy is extracted via the following equation analytically at different coverages (Eq. (4)).

$$\frac{E_d}{k_B T_p} = \ln\left(\frac{k_o T_p n \theta^{n-1}}{\beta_H}\right) - \ln\left(\frac{E_d}{k_B T_p}\right) \quad (4)$$

T_p is the maximum peak temperature and k_B is Boltzmann constant, $8.61 \times 10^{-5} \text{ eV K}^{-1}$.

If the desorption is not an activated process the adsorption energy

would be the negative of the desorption energy, then one may divide it into two parts. At very low coverage this energy would be that of true nearly isolated molecules on the surface while at high coverage the energy decreases due to interaction of the adsorbates. The difference in energy of about a quarter between near 0.06 and 1 may then be

attributed to the interaction (repulsive) energy.

4. Acetaldehyde and ethylene formation and desorption

Fig. 3B shows acetaldehyde desorption (m/e 29) at different coverages. The desorption temperature at 600–650 K is much higher than that of a molecularly adsorbed/desorbed acetaldehyde [35] on UO₂ (or acetaldehyde TPD of other oxides [36–42]). Carbonyl compounds (because they adsorb molecularly on a metal oxide surface in an η^1

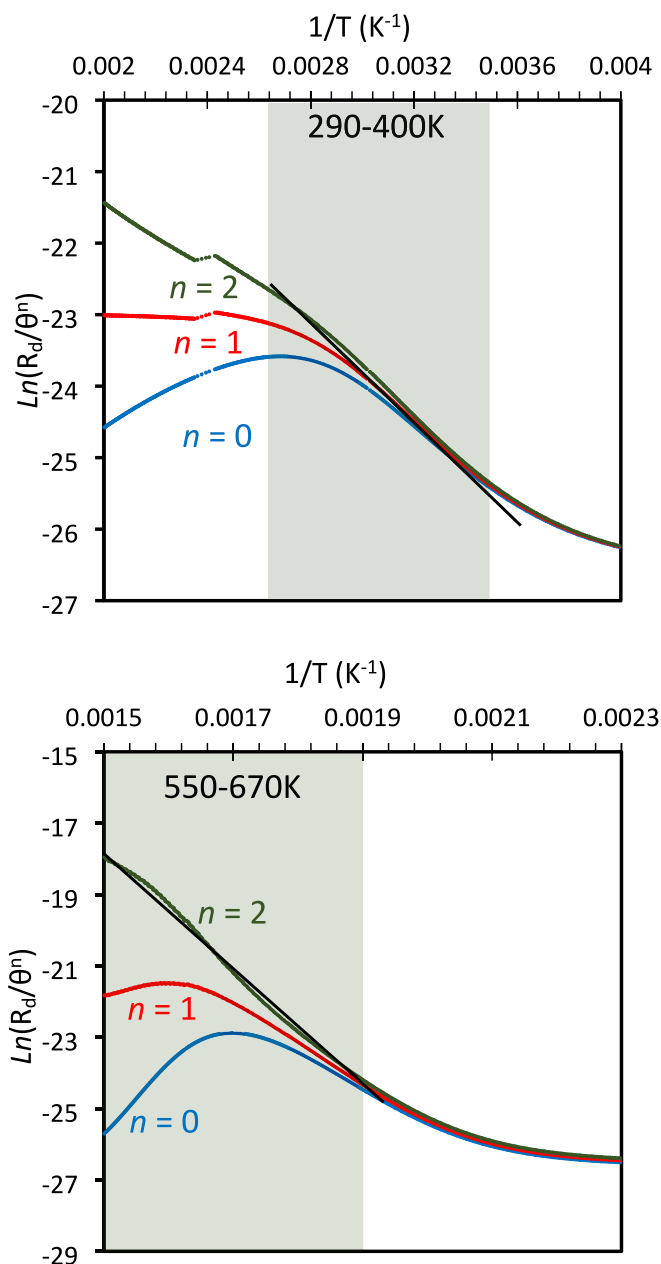


Fig. 4. Fitting of the effect of desorption order (n) on the desorption rate during ethanol-TPD on a UO_2 thin film in the two temperature domains (290–400 K and 550–670 K).

configuration via their oxygen lone pair [43,44] have weaker adsorption energies [45–47] than dissociatively adsorbed alcohols [48–51]. The desorption is therefore reaction-limited as described by scheme 1 below (and equation 5).

Ethoxide dehydrogenation



Dissociatively adsorbed ethanol

Acetaldehyde + Hydrogen + site regeneration

Table 3

Effect of surface coverage on the desorption energy of Peak 1 during ethanol-TPD on a UO_2 thin film.

Coverage θ	Temperature (K)	Desorption energy, E_d	Desorption energy, E_d
		(kJ/mol) $n = 1$	(kJ/mol) $n = 2$
0.06	505	136	127
0.08	482	129	122
0.31	463	124	122
0.41	438	117	117
0.54	400	107	107
1	377	100	103

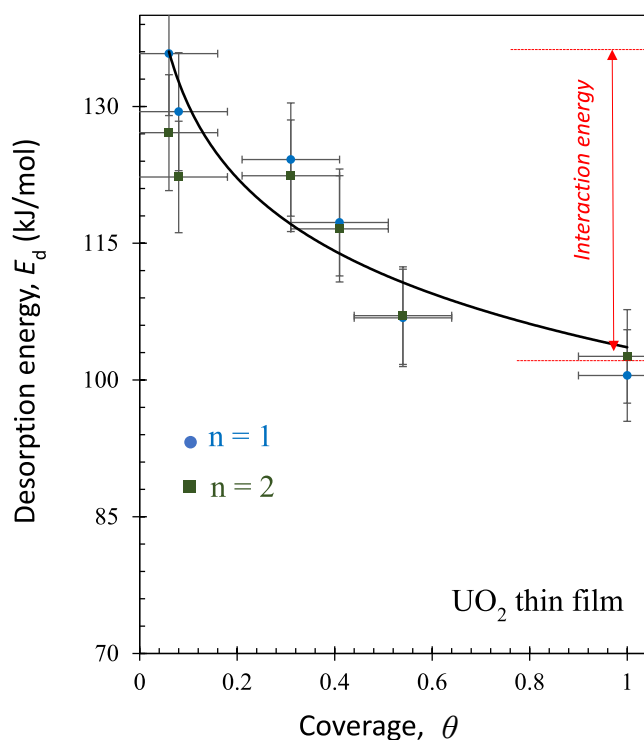
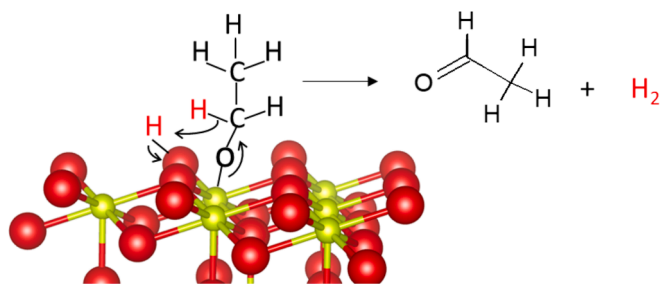


Fig. 5. Ethanol desorption energy in the 370–500 K temperature range as a function of surface coverage during TPD. The desorption energy is computed using equation (4).

–U–O– represents the sites for the dissociative adsorption.

This reaction, known as beta-hydride elimination, as per its name, involves the removal of a H ion plus two electrons (a hydride) from the carbon atom adjacent to the O atom of the alkoxide. This hydride combines with the proton of the surface hydroxyl, also adjacent to it, to release a hydrogen molecule. The reaction, in this work, appears however to respond to the initial surface coverage of ethanol as seen by the shift in desorption temperature from 640 K at $\theta = 0.06$ to 610 K at full



Scheme 1. A schematic representation of the dehydrogenation of a dissociatively adsorbed ethanol molecule on $\text{UO}_2(1\ 1\ 1)$ surface to acetaldehyde and hydrogen molecules observed to desorb at 610–640 K during ethanol-TPD. Yellow (small) balls: U^{4+} cations. Red (large) balls: O^{2-} anions. The arrows indicate the direction of electron transfer during the reaction/desorption step.

coverage. Inspection of the desorption profile indicated that the FWHM of the peaks is about the same at the investigated coverages and therefore the shift is not due to multiple desorption (multiple channels) with



Dissociatively adsorbed ethanol *Ethylene + water + site regeneration*

(6)

increasing coverage. On the contrary, ethanol re-combinative desorption at the same temperature domain does not shift with increasing coverage. Since ethanol desorption, at this temperature domain, does not shift to lower temperatures with increasing coverage while that of the dehydrogenation shifts, one may conclude that the possible repulsive interaction between adsorbates at high coverage affects the dehydrogenation reaction but not the protonation reaction.

A third reaction is also seen and it involves the formation of ethylene, by the dehydration of the dissociatively adsorbed ethanol, as seen in

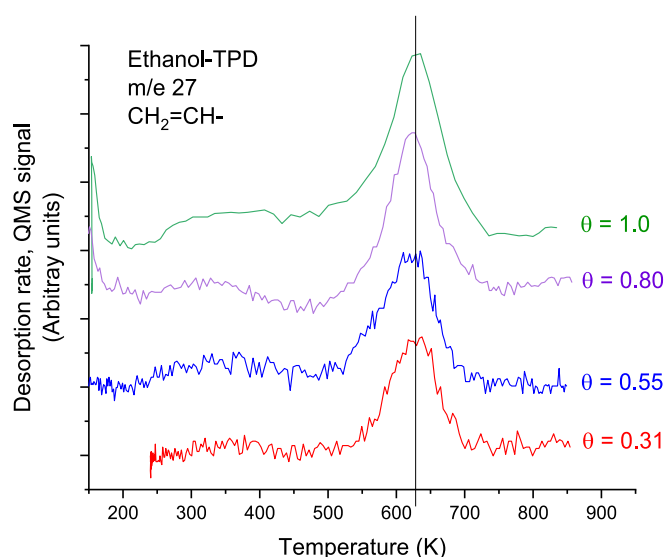


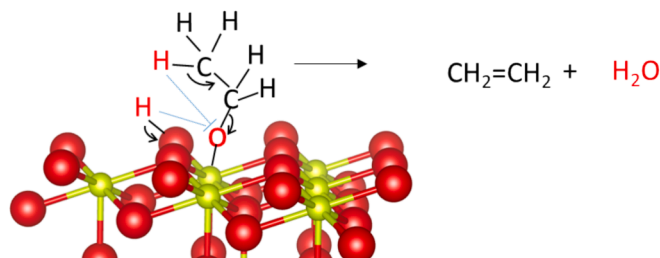
Fig. 6. Ethylene desorption at different initial surface coverage of ethanol-TPD on a UO_2 thin film. Ethanol ($m/e\ 31 \times 0.1$) and acetaldehyde contribution ($m/e\ 29 \times 0.05$) were subtracted. $m/e\ 26$ is preferred instead of $m/e\ 27$ for ethylene as it has less contribution from ethanol and acetaldehyde fragments.

Fig. 6. This is also a common reaction of primary and secondary alcohols. Many attempts in the past have been made to study the factors behind the selectivity of these two reaction products: dehydrogenation to acetaldehyde (an aldehyde) and dehydration to ethylene (an olefin). Observations indicate that oxides [52,53] such as Al_2O_3 , V_2O_5 , MoO_3 and WO_3 favor a dehydration reaction while oxides such as CeO_2 , [54,55] and CuO [56] orient towards dehydrogenation reaction. However, most oxides also give both products. The dehydration reaction appears to have more steps than the dehydrogenation step as it involves the breaking of an sp^3 terminal C–H atom, of a carbon–oxygen bond, and consequently the formation of a double bond via an intra-molecular rearrangement. One of the obvious main differences between both reactions is that ethoxides to acetaldehyde involve the breaking of one bond in the adsorbed species, this is a H–C bond where the H atoms depart as a hydride while that to ethylene involves the breaking of two bonds; a H–C bond in which H departs as a proton and a C–O bond. Ethylene with a negligible heat of adsorption on an oxide would desorb instantaneously upon formation. The temperature is also high enough to desorb water formed during the reaction.

Ethoxide dehydration

$-\text{U}-\text{O}-$ represents the sites for the dissociative adsorption.

Why a surface orients toward dehydration instead of dehydrogenation of an adsorbed alcohol has been the topic of many experimental (as mentioned above) and theoretical [57,58] works. Both products desorb at the same temperature (during TPD) and while they may change in selectivity during a steady-state reaction with temperature [56] this change is mild when a comparison is made between many oxides. Irrespective of the rearrangement of the species before and during the reaction (as represented in Schemes 1 And 2) the dehydrogenation reaction results in a carbonyl formation ($-\text{C}=\text{O}$) which has a much weaker adsorption energy when compared to an alkoxy ($\text{R}-\text{O}(\text{a})$) and therefore desorb. The dehydration reaction results in an olefin ($-\text{C}=\text{C}-$) which has very weak adsorption [59,60] than a carbonyl compound on oxides. Therefore, the selectivity is largely independent from the heat of adsorption/desorption of the reaction products. There is however one factor that might have an effect. The stoichiometric



Scheme 2. A schematic representation of the dehydration of a dissociatively adsorbed ethanol molecule on $\text{UO}_2(1\ 1\ 1)$ surface to ethylene and water molecules observed to desorb at ca. 630 K K during Ethanol-TPD. Yellow (small) balls: U^{4+} cations. Red (large) balls: O^{2-} anions. The arrows indicate the direction of electron transfer during the reaction/desorption step. The blue dashed lines represent an interaction between the H atoms and one of the two lone pair orbitals of oxygen of the alkoxy.

Table 4

Acetaldehyde to ethylene ratio during ethanol-TPD as a function of surface coverage.

Ethanol exposure (L)	m/e ratio* (29/26) Acetaldehyde/Ethylene
0.18	0.87
0.31	0.71
0.31	0.81
0.55	1.05
0.80	0.75
1.0	0.62
	(average) 0.78

* The contribution of the fragmentation patterns of ethanol in the peak area of m/e 29 (–CHO) and m/e 26 (–CH = CH–) was subtracted.

(complementary) reaction products are hydrogen (in the case of the aldehyde) and water (in the case of the olefin). Therefore, the interaction of the precursor of these reaction products may affect the selectivity. In the case of ethylene formation, there is the possibility that the fragment containing the water molecule formed being delayed from desorption and therefore ethylene formation and desorption will be delayed. If this is the case then the affinity of a metal cation to the oxygen of the adsorbate may affect the reaction selectivity. In previous works, a relationship between the heat of formation of oxides, their dielectric constants, as well as their Madelung potential correlated well with the selectivity of acetaldehyde to ethylene. The ratio of these two products of about 0.8 (Table 4) in this work is very similar to that found on a UO₂(1 1 1) single crystal previously. It is far lower than that of ZnO (0001) single crystal [61], or polycrystalline [62] CeO₂, both oxides are considered ionic and basic (alkaline) oxides [63–65], and similar to that of the more covalent [66–68], TiO₂. This is consistent with the nature of the bonding where both U–O and Ti–O have a nonnegligible covalent fraction. It is also apparent that this ratio is not much affected by surface coverage as shown in Table 4.

5. Conclusions

Two modes of adsorptions/desorptions for ethanol on a UO₂ thin film were identified by temperature programmed desorption. The molecular adsorption, that was sensitive to surface coverage, largely desorb in the 250–500 K region with desorption energies (E_d) ranging between 100 and 130 kJ/mol. A second desorption channel at ca. 630 K (E_d = ca. 150 kJ/mol) was not sensitive to surface coverage and is attributed to surface ethoxide re-combinative desorption. The second desorption channel is accompanied by the desorption of the two main reaction products: the dehydrogenation product acetaldehyde, and the dehydration product ethylene. The molar ratio of these two products is sensitive to the nature of the chemical and structural bonding of a binary metal oxide. A high ratio is often found for basic oxides while a low ratio, often less than 1, for oxides with a high contribution of covalent bonding between the metal cation and the oxygen anion. The molar ratio of these two products of 0.8 was almost the same to that previously found on a UO₂(1 1 1) single crystal, and in line with the U–O bonding nature that contains a non-negligible fraction of covalency, like TiO₂ and other amphoteric oxides.

CRedit authorship contribution statement

Hicham Idriss: Writing – review & editing, Writing – original draft, Methodology, Investigation, Formal analysis. **Thomas Gouder:** Investigation.

Declaration of competing interest

The authors declare that they have no known competing financial interests or personal relationships that could have appeared to influence the work reported in this paper.

Acknowledgments

The authors thank Mr. Frank Huber for his technical assistant throughout the study and Dr. Rachel Eloirdy for her managerial support.

Data availability

Data will be made available on request.

References

- [1] M.A. Barteau, Organic reactions at well-defined oxide surfaces, *Chem. Rev.* 96 (1996) 1413–1430.
- [2] A. Dey, Semiconductor metal oxide gas sensors: A review, *Mater. Sci. Eng. B* 229 (2018) 206–217.
- [3] P. Silva-Bermudez, S.E. Rodil, An overview of protein adsorption on metal oxide coatings for biomedical implants, *Surf. Coatings Technol.* 233 (2013) 147–158.
- [4] A. Hussain, F. Rehman, H. Rafeeq, M. Waqas, A. Asghar, N. Afshen, A. Rahdar, M. Bilal, H.M.N. Iqbal, In-situ, Ex-situ, and nano-remediation strategies to treat polluted soil, water, and air—A review, *Chemosphere* 289 (2022) 133252.
- [5] S.R. Egorova, R.R. Tuktarov, A.V. Boretskaya, A.I. Laskin, R.N. Gizyatullo, A. A. Lamberov, Stabilizing effect of α -Cr₂O₃ on highly active phases and catalytic performance of a chromium alumina catalyst in the process of isobutane dehydrogenation, *Mol. Catal.* 509 (2021) 111610.
- [6] A. Trovarelli, Catalytic properties of ceria and CeO₂-containing materials, *Catal. Rev.* 38 (4) (1996) 439–520.
- [7] I. P. Prosvirnin, E. P. Tikhomirov, A. M. Sorokin, V. V. Kaichev, and V. I. Bukhtiyarov, In Situ Study of the Selective Oxidation of Methanol to Formaldehyde on Copper, *Kinet. & Catal.* 44, (2003) 662–668. Translated from *Kinetika i Kataliz* 44 (2003) 724–730.
- [8] M. Karatok, M.G. Sensoy, E.I. Vovk, H. Ustunel, D. Toffoli, E. Ozensoy, Formaldehyde selectivity in methanol partial oxidation on silver: Effect of reactive oxygen species, surface reconstruction, and stability of intermediates, *ACS Catal.* 11 (2021) 6200–6209.
- [9] A. Cross, S. Roslyakov, K.V. Manukyan, S. Rouvimov, A.S. Rogachev, D. Kovalev, E. E. Wolf, A.S. Mukasyan, In situ preparation of highly stable ni-based supported catalysts by solution combustion synthesis, *J. Phys. Chem. C* 118 (2014) 26191.
- [10] K.V. Manukyan, A.J. Cross, A.V. Yeghishyan, S. Rouvimov, J.J. Miller, A. S. Mukasyan, E.E. Wolf, Highly stable Ni–Al₂O₃ catalyst prepared from a Ni–Al layered double hydroxide for ethanol decomposition toward hydrogen, *Appl. Catal. A: General* 508 (2015) 37–44.
- [11] V. Fung, M. Janik, S. Crossley, Y.-H.-C. Chin, A. Savara, Toward understanding and controlling organic reactions on metal oxide catalysts, *J. Phys. Chem. C* 127 (2023) 13451–13465.
- [12] H. Idriss, Surface reactions of uranium oxide powder, thin films and single crystals, *Surf. Sci. Reports* 65 (2010) 67–109.
- [13] S.K. Potts, P. Kegler, S. Hammerich, M. Klinkenberg, I. Niemeyer, D. Bosbach, S. Neumeier, Long-term stability of uranium-oxide-based microparticle reference materials: Shelf-life in alcoholic suspension and storage media, *MRS Adv.* 7 (2022) 134–139.
- [14] R. Middendorp, M. Klinkenberg, M. Dürr, Uranium oxide microparticle suspensions for the production of reference materials for micro-analytical methods, *J. Radioanal. Nucl. Chem.* 318 (2018) 907–914.
- [15] L.E. Roy, T. Durakiewicz, R.L. Martain, J.E. Peralta, G.E. Scuseria, C.G. Olson, J. J. Joyce, E. Guzewicz, Dispersion in the Mott insulator UO₂: A comparison of photoemission spectroscopy and screened hybrid density functional theory, *J. Comput. Chem.* 29 (2008) 2288–2294.
- [16] O.T. Summerscales, F. Geoffrey, N. Cloke, P.B. Hitchcock, J.C. Green, N. Hazar, Reductive cyclotrimerization of carbon monoxide to the delatate dianion by an organometallic uranium complex, *Science* 331 (2006) 829.
- [17] P.O. Alfaro, J.H. Torres, F.P. Thiele, Reduction kinetics of uranium trioxide to uranium dioxide using hydrogen, *World J. Nucl. Sci. Technol.* 5 (2015) 149–156.
- [18] H. Madhavaram, H. Idriss, Carbon efficiency and the surface chemistry of the actinides: direct formation of furan from acetylene over β -UO₃, *J. Catal.* 206 (2002) 155–158.
- [19] G. El Jamal, T. Gouder, R. Eloirdy, E. Tereshina-Chitrova, L. Horádk, M. Jonsson, Mixed H₂O/H₂ plasma-induced redox reactions of thin uranium oxide films under UHV conditions, *Dalton Trans.* 50 (2021) 12583–12591.
- [20] S.V. Chong, T.R. Griffiths, H. Idriss, Ethanol reactions over the UO₂(111) single crystal: effect of the Madelung potential on the reaction selectivity, *Surf. Sci.* 444 (2000) 187–198.
- [21] M.A. Nadeem, G.I.W. Waterhouse, H. Idriss, The reactions of ethanol on TiO₂ and Au/TiO₂ anatase catalysts, *Catal. Today* 182 (2012) 16–24.
- [22] E.I. Ko, J.B. Benziger, R.J. Madix, Reactions of methanol on W (100) and W (100)-(5 × 1) C surfaces, *J. Catal.* 62 (1980) 264–274.
- [23] P.Y. Sheng, G.A. Bowmaker, H. Idriss, The reactions of ethanol over Au/CeO₂, *Appl. Catal. A* 261 (2004) 171–181.
- [24] A. De Jong, J. Niemantsverdriet, Thermal desorption analysis: Comparative test of ten commonly applied procedures, *Surf. Sci.* 233 (1990) 355–365.
- [25] R.I. Masel, Principles of Adsorption and Reaction on Solid Surfaces, John Wiley & Sons Inc, 1996.
- [26] G. El Jamal, T. Gouder, R. Eloirdy, H. Idriss, M. Jonsson, Study of water interaction with UO₂, U₂O₅, and UO₃: tracking the unexpected reduction of uranium cations

- and characterization of surface-bound hydroxyls, *J. Phys. Chem. C* 127 (2023) 14222–14231.
- [27] G. El-Jamal, T. Gouder, R. Eloirdi, M. Jonson, H. Idriss, Monitoring the reduction of UO_3 thin film by hydrogen atoms using valence-level spectroscopy: correlating the U5f^6 signal to surface hydroxyls, *Frontiers in Fuels. Sec. Non-Carbon-Based Fuels 1* (2023) – no page number.
- [28] H. Idriss, On the wrong assignment of the XPS O1s signal at 531–532 eV attributed to oxygen vacancies in photo- and electro-catalysts for water splitting and other materials applications, *Surf. Sci.* 712 (2021) 121894.
- [29] C.L. Dugan, G.G. Peterson, A. Mock, C. Young, J.M. Mann, M. Nastasi, M. Schubert, L. Wang, W.-N. Mei, I. Tanabe, P.A. Dowben, J. Petrosky, Electrical and material properties of hydrothermally grown single crystal (111) UO_2 , *Eur. Phys. J. B* 91 (2018) 67.
- [30] T.T. Meek, B. von Roedern, P.G. Clem, R.J. Hanrahan Jr., Some optical properties of intrinsic and doped UO_2 thin films, *Mater. Lett.* 59 (2005) 1085–1088.
- [31] E. Enriquez, G. Wang, Y. Sharma, I. Sarpkaya, Q. Wang, D. Chen, N. Winner, X. Guo, J. Dunwoody, J. White, A. Nelson, H. Xu, P. Dowden, E. Batista, H. Htoon, P. Yang, Q. Jia, A. Chen, Structural and optical properties of phase-pure UO_2 , $\alpha\text{-U}_3\text{O}_8$, and $\alpha\text{-UO}_3$ epitaxial thin films grown by pulsed laser deposition, *ACS Appl. Mater. Interf.* 12 (2020) 35232–35241.
- [32] L. Gamble, L.S. Jung, C.T. Campbell, Decomposition and protonation of surface ethoxys on TiO_2 (110), *Surf. Sci.* 348 (1995) 1–16.
- [33] A.M. Nadeem, J.M.R. Muir, K.A. Connelly, B.T. Adamson, J. Metson, H. Idriss, Ethanol photo-oxidation on a rutile TiO_2 (110) single crystal surface, *PCCP* 13 (2011) 7637–7643.
- [34] P.M. Jayaweera, E.L. Quah, H. Idriss, Photoreaction of ethanol on TiO_2 (110) single-crystal surface, *J. Phys. Chem. C* 111 (2007) 1764–1769.
- [35] S.V. Chong, H. Idriss, Reactions of acetaldehyde on UO_2 (111) single crystal surfaces. evidence of benzene formation, *J. Vac. Sci. Technol. A* 19 (2001) 1933.
- [36] H. Madhavaram, H. Idriss, Acetaldehyde reactions over the uranium oxide system, *J. Catal.* 224 (2004) 358–369.
- [37] J. Raskó, J. Kiss, Adsorption and surface reactions of acetaldehyde on TiO_2 , CeO_2 and Al_2O_3 , *Appl. Catal. A: General* 287 (2005) 252–260.
- [38] H. Idriss, K.S. Kim, M.A. Barteau, Carbon-carbon bond formation via aldolization of acetaldehyde on single crystal and polycrystalline TiO_2 surfaces, *J. Catal.* 139 (1993) 119–133.
- [39] H. Idriss, C. Diagne, J.P. Hindermann, A. Kiennemann, M.A. Barteau, Reactions of acetaldehyde on CeO_2 and CeO_2 -supported catalysts, *J. Catal.* 155 (1995) 219–237.
- [40] P.-M. Albrecht, D.R. Mullins, Acetaldehyde adsorption and reaction on CeO_2 (100) thin films, *J. Phys. Chem. C* 113 (2013) 14692–14700.
- [41] H. Madhavaram, H. Idriss, Temperature programmed desorption of ethylene and acetaldehyde on uranium oxides. Evidence of furan formation from ethylene, *Stud. Surf. Sci. Catal.* 110 (1997) 265–274.
- [42] M.J. Rasmussen, S. Najmi, G. Innocenti, A.J. Medford, C. Sievers, J.W. Medlin, Supported molybdenum oxides for the aldol condensation reaction of acetaldehyde, *J. Catal.* 408 (2022) 216–226.
- [43] J. Raskó, T. Kecskés, J. Kiss, FT-IR and mass spectrometric studies on the interaction of acetaldehyde with TiO_2 -supported noble metal catalysts, *Appl. Catal. A: General* 287 (2005) 244–251.
- [44] M. Singh, N. Zhou, D.K. Paul, K.J. Klabunde, *J. Catal.* 260 (2008) 371–379.
- [45] T. Würger, W. Heckel, K. Sellschopp, S. Müller, A. Stierle, Y. Wang, H. Noei, G. Feldbauer, Adsorption of acetone on rutile TiO_2 : A DFT and FTIR study, *J. Phys. Chem. C* 122 (2018) 19481–19490.
- [46] J.M.R. Muir, H. Idriss, Formaldehyde adsorption geometry and energies over TiO_2 (1 1 0) rutile surface, *Chem. Phys. Lett.* 572 (2013) 125–129.
- [47] K. Katsiev, G. Harrison, H. Alghamdi, Y. Alsalik, A. Wilson, G. Thornton, H. Idriss, Mechanism of ethanol photooxidation on single-crystal anatase TiO_2 (101), *J. Phys. Chem. C* 121 (2017) 2940–2950.
- [48] H. Alghamdi, H. Idriss, Study of the modes of adsorption and electronic structure of hydrogen peroxide and ethanol over TiO_2 rutile (110) surface within the context of water splitting, *Surf. Sci.* 669 (2018) 103–113.
- [49] V. Orazi, A. Juan, E.A. González, Jorge M. Marchetti, P.V. Jasen, DFT study of ethanol adsorption on CaO (0 0 1) surface, *Appl. Surf. Sci.* 500 (2020) 144254.
- [50] C. Rohmann, H. Idriss, A computational study of the interaction of oxygenates with the surface of rutile TiO_2 (110). Structural and electronic trends, *J. Phys.: Cond. Matt.* 34 (2022) 154002.
- [51] H.-N. Chiang, S. Nachimuthu, Y.-C. Cheng, N.P. Damayanti, J.-C. Jiang, A DFT study of ethanol adsorption and decomposition on $\alpha\text{-Al}_2\text{O}_3$ (0001) surface, *Appl. Surf. Sci.* 363 (2016) 636–643.
- [52] J. Cunningham, B.K. Hodnett, M. Ilyas, J. Tobin, E.L. Leahy, Dehydrogenation versus dehydration of aliphatic alcohols on metal oxides, *Faraday Discuss. Chem. Soc.* 72 (1981) 283–302.
- [53] R. Rousseau, D.A. Dixon, B.D. Kay, Z. Dohnálek, Dehydration, dehydrogenation, and condensation of alcohols on supported oxide catalysts based on cyclic $(\text{WO}_3)_3$ and $(\text{MoO}_3)_3$ clusters, *Chem. Soc. Rev.* 43 (2014) 7664.
- [54] A. Salcedo, E. Poggio-Fraccari, F. Mariño, B. Irigoyen, Tuning the selectivity of cerium oxide for ethanol dehydration to ethylene, *Appl. Surf. Sci.* 599 (2022) 153963.
- [55] S. Tayrabekova, P. Mäki-Arvela, M. Peurla, P. Paturi, K. Eränen, G.E. Ergazieva, A. Aho, D.Y. Murzin, K. Dossunov, Catalytic dehydrogenation of ethanol into acetaldehyde and isobutanol using mono-and multicomponent copper catalysts, *Compt. Rend. Chim.* 21 (2018) 194–209.
- [56] G. Pampararo, G. Garbarino, P. Riani, M. Villa García, V.S. Escribano, G. Busca, A study of ethanol dehydrogenation to acetaldehyde over supported copper catalysts: catalytic activity, deactivation and regeneration, *Appl. Catal. A, General* 602 (2020) 117710.
- [57] J. Pang, M. Yin, P. Wu, X. Li, H. Li, M. Zheng, T. Zhang, Advances in catalytic dehydrogenation of ethanol to acetaldehyde, *Green Chem.* 23 (2021) 7902–7916.
- [58] P. Kostestky, J. Yu, R.J. Gorte, G. Mpourmpakis, Structure–activity relationships on metal-oxides: alcohol dehydration, *Catal. Sci. Technol.* 4 (2014) 3861–3869.
- [59] G. Shukri, H. Kasai, Density functional theory study of ethylene adsorption on clean anatase TiO_2 (001) surface, *Surf. Sci.* 619 (2014) 59–66.
- [60] C.-F. Mao, M.A. Vannice, High surface area α -alumina. I: Adsorption properties and heats of adsorption of carbon monoxide, carbon dioxide, and ethylene, *Appl. Catal. A: General* 111 (1994) 151–173.
- [61] J.M. Vohs, M.A. Barteau, Dehydration and dehydrogenation of ethanol and 1-propanol on the polar surfaces of zinc oxide, *Surf. Sci.* 221 (1989) 590–608.
- [62] A. Yee, S. Morrison, H. Idriss, A study of the reactions of ethanol on CeO_2 and Pd/ CeO_2 by steady state reactions, temperature programmed desorption, and in situ FT-IR, *J. Catal.* 186 (1999) 279–295.
- [63] C. Zhou, L.Z. Sun, X.L. Zhong, X. Chen, L. Wei, J.B. Wang, First-principle study on bonding mechanism of ZnO by LDA+U method, *Phys. Lett. A* 368 (2007) 112–116.
- [64] K.I. Maslakov, Y.A. Teterin, M.V. Ryzhkov, A.J. Popel, A.Y. Teterin, K.E. Ivanov, S. N. Kalmykov, V.G. Petrov, P.K. Petrov, I. Farnan, The electronic structure and the nature of the chemical bond in CeO_2 , *PCCP* 20 (2018) 16167–16175.
- [65] H. Nakamatsu, T. Mukoyama, H. Adachi, Ionic and covalent bonds in CeO_2 crystal, *Chem. Phys. Lett.* 247 (1995) 168–172.
- [66] B. Jiang, J.M. Zuo, N. Jiang, M. O’Keefe, J.C.H. Spence, Charge density and chemical bonding in rutile, TiO_2 , *Acta Cryst. A* 59 (2003) 341–350.
- [67] C. Sousa, F. Illas, Ionic-covalent transition in titanium oxides, *Phys. Rev. B* 50 (1994) 13974.
- [68] K.S. Kim, M.A. Barteau, Reactions of aliphatic alcohols on the {011}-faceted TiO_2 (001) surface, *J. Mol. Catal.* 63 (1990) 103–117.